# Cryogenic beam-combiner for very low background, 2-20 micron interferometry on the 22.8 m Large Binocular Telescope

D.W. McCarthy[a], E. Sabatke[b], R. Sarlot[a], P. Hinz[a], and J. Burge[a,b]

[a]Steward Observatory, 933 N. Cherry Ave., Tucson, AZ, USA 85721

[b]Optical Sciences Center, 1630 E. University Blvd., Tucson, AZ, USA 85721

## ABSTRACT

The 22.8 m Large Binocular Telescope Interferometer will be a uniquely powerful tool for imaging and nulling interferometry at thermal infrared wavelengths (2-20 $\mu$m) because of the LBT's unusual combination of low emissivity, high spatial resolution, broad (u,v)-plane coverage, and high photometric sensitivity. The Gregorian adaptive secondary mirrors permit beam combination after only three warm reflections. They also control the relative pathlength, wavefront tip/tilt, and focus of the two telescope beams, thus greatly simplifying the complexity of the beam-combiner. The resulting four-mirror beam-combiner reimages the original focal plane and also images the telescope pupil onto a cold stop to limit thermal background. At first-light in 2004, an all-reflective, cooled beam-combiner can provide a 2 arcmin diameter field for Fizeau-style imaging as well as the low thermal background and achromaticity required for nulling interferometry. In designing the optics of such a beam-combiner, we can maximize the field of view at the combined focus by balancing the competing effects of differential phase, tilt, distortion, focus, and pupil matching. To achieve a "peak Strehl" of 0.9 at a wavelength of 4.8$\mu$m across a 1.0 arcmin field radius, strong constraints are placed on differential image overlap (~0.03 arcsec), single beam distortion (0.1%), and pupil matching (0.1%). This cryogenic beam-combiner can feed a variety of interchangeable cameras and spectrographs. Tip/tilt and pathlength (phase) sensors near the final focus within each science instrument will control the adaptive secondaries to maintain precise alignment and provide the highest possible Strehl ratio.

**Keywords:** Interferometry, infrared, LBT, nulling

## 1. INTRODUCTION

The Large Binocular Telescope Interferometer (LBTI) is a versatile tool for high angular resolution imaging, interferometry, and spectroscopy. Providing images ten times sharper than the Hubble Space Telescope with a collecting area 24 times larger, the LBT's entrance pupil also offers broader coverage of the (u,v)-plane and a wider field of view than other interferometers. Hill & Salinari (2000) discuss the present status of the overall LBT. Its use as an imaging and nulling interferometer has been addressed previously by Angel et al. (1998) and Hill (1994).

Although it can be operated at wavelengths from the ultraviolet to the sub-millimeter, the LBT is uniquely powerful in the thermal infrared. Its relatively simple, co-mounted optics and adaptive secondary mirrors provide low thermal background and high throughput. Lloyd-Hart (2000) has shown that these aspects enable the LBT to outperform other large telescopes by factors of 3-5× in the integration time required to detect a background-limited source. When used as a nulling interferometer (Hinz et al. 1998; Hinz et al. 2000), the LBT will be unsurpassed in its sensitivity to circumstellar sources such as zodiacal dust clouds and Jovian-like planets. Because of the relative closeness of its primary mirrors, an LBT nulling interferometer reduces the leak from a central star to 0.01%, about 35 times better than achieved with the more widely spaced Keck Interferometer.

Beginning at first-light in 2004, we wish to capitalize on the LBT's performance at wavelengths from 2-20 $\mu$m. For this purpose we are designing an all-reflective beam-combiner with moderate field and versatility for scientific imaging and spectroscopy. Here we explore realistic optical designs to maximize the interferometrically combined

Further author information: (Send correspondence to DM)
DM: E-mail: dmccarthy@as.arizona.edu
ES: E-mail: esabatke@optics.arizona.edu
RS: E-mail: rsarlot@as.arizona.edu
PH: E-mail: phinz@as.arizona.edu
JB: E-mail: jburge@as.arizona.edu

In *Interferometry in Optical Astronomy*, Pierre J. Léna, Andreas Quirrenbach, Editors,
Proceedings of SPIE Vol. 4006 (2000) • 0277-786X/00/$15.00

**Figure 1.** Surface plot of the on-axis, unaberrated PSF at the combined focus of the LBT at 4.8$\mu$m.The envelope of a single beam Airy pattern, 0.29 arcsec, is modulated by fringes of width, 0.069 arcsec.

field of view, establishing a merit function based on tolerances for differential phase, tilt, distortion, focus, and pupil matching between the two interfering telescope beams. This work is inspired by previous studies (Byard & Bonacinni 1994; Salinari 1996) which analyzed potential beam-combining methods but did not model the interferometrically combined field or consider opto-mechanical manufacturing and alignment tolerances.

In parallel with this study, Herbst et al. (2000) consider a beam-combiner design for shorter wavelengths and Walker et al. (2000) present a design for the sub-millimeter.

## 2. THEORETICAL ANALYSIS OF AN LBT INTERFEROMETER SYSTEM

To aid in comparing the performance of various beam-combiner designs, we have considered different practical merit functions. For maximum benefit, a useful merit function should quantify a system's point-spread-function (PSF) as a function of field angle. To determine which merit function would be most beneficial, we have studied the LBTI's point spread function in the presence of different aberrations.

In the remainder of this paper all Strehl ratios refer to the interferometrically combined focal plane.

### 2.1. Unaberrated PSF Behavior of the LBTI

There are three basic elements to the LBTI's theoretical point spread function: two diffraction-limited Airy patterns, one from each telescope, and a cosine pattern from the interference of the two beams. The cosine pattern has an envelope whose width depends on the spectral bandwidth. The final PSF is the sum of the Airy patterns, multiplied by the cosine pattern. When all three components are centered at the same point anywhere in space, the PSF has a theoretical maximum. A completely unaberrated PSF is shown in Figure 1. Figure 2 illustrates density plots of the unaberrated PSF and MTFs.

### 2.2. Aberrated PSF Behavior of the LBTI

The effects of first-order aberrations were modeled at a wavelength of 4.8$\mu$m with a total bandwidth of 1.2$\mu$m, somewhat broader than the classical $M$-band. Piston, tilt, and defocus errors were considered in one of the primary apertures for on-axis imaging. Higher-order aberrations were not considered, since they would only reduce the theoretical maximum by driving light out of the center of the Airy pattern.

Figure 3 shows the PSF's of the LBTI in the presence of a piston (constant phase) error in one aperture for the on-axis case. The corresponding MTFs are also shown. Because the coherence length is 19.2$\mu$m, the unaberrated pattern should devolve with increasing piston into the simple superposition of the two Airy patterns, reducing the maximum of the PSF by a factor of two.

Figure 4 shows the effects of tilt errors where one image is moved perpendicular to the baseline direction. This tilt error effectively shifts the corresponding Airy pattern without affecting the location of the other Airy pattern and cosine envelope. The peak of the PSF should then decrease with an Airy-squared profile, as the Airy patterns

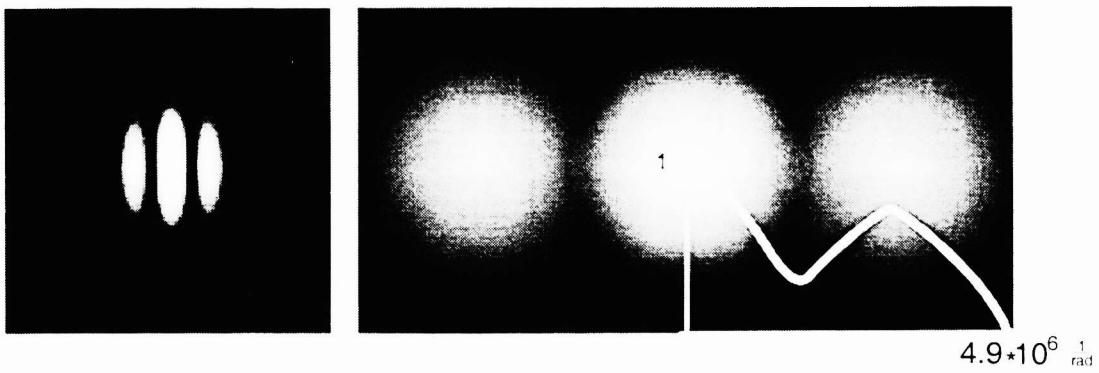


**Figure 2.** Density plots of the square-roots of the unaberrated PSF (left) and MTF at the combined focus of the LBT at 4.8$\mu$m. The superimposed graph at the right is a horizontal cut through the center of the MTF.

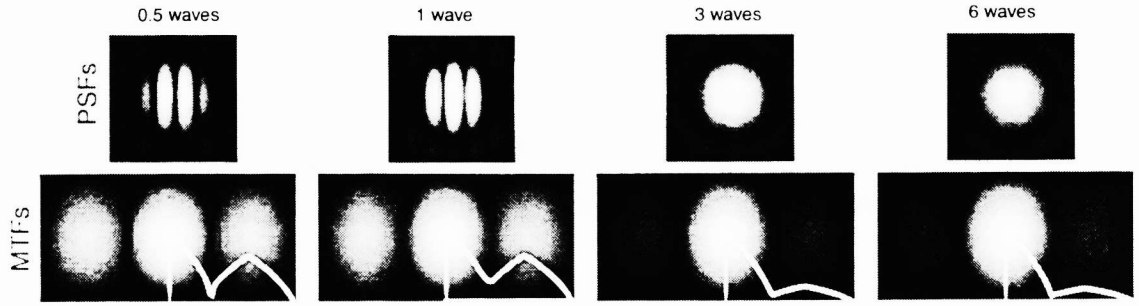


**Figure 3.** Point spread functions of the LBTI vs. piston (constant phase) error in one telescope beam at 4.8$\mu$m. The corresponding MTFs are shown in the lower panel.

separate, with a final PSF height reduced by a factor of four when the Airy patterns are completely separated. The modulation transfer function (MTF) narrows as the width of the PSF increases, and fringes appear due to the double-aperture nature of the PSF.

Figure 5 illustrates the effect of a tilt error where one image is moved along the baseline direction. Similar to the previous case, one of the Airy patterns is moving away from the location of the cosine envelope and second Airy pattern. In this case, however, the peak of the PSF should fall off more quickly, since the Airy pattern is moving perpendicular to the cosine fringes. Again, the width of the MTF decreases as the PSF width increases, and fringes appear, perpendicular to the fringe direction of the previous case.

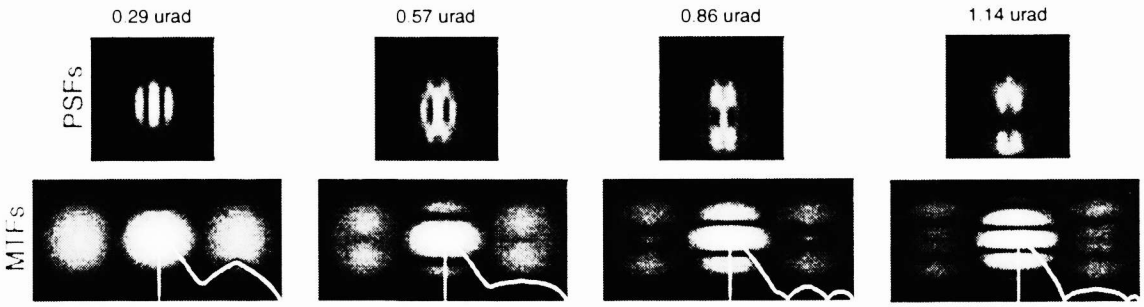


**Figure 4.** Point spread functions of the LBTI vs. tilt error perpendicular to the baseline direction for one telescope beam at 4.8$\mu$m. The corresponding MTFs are shown in the lower panel.

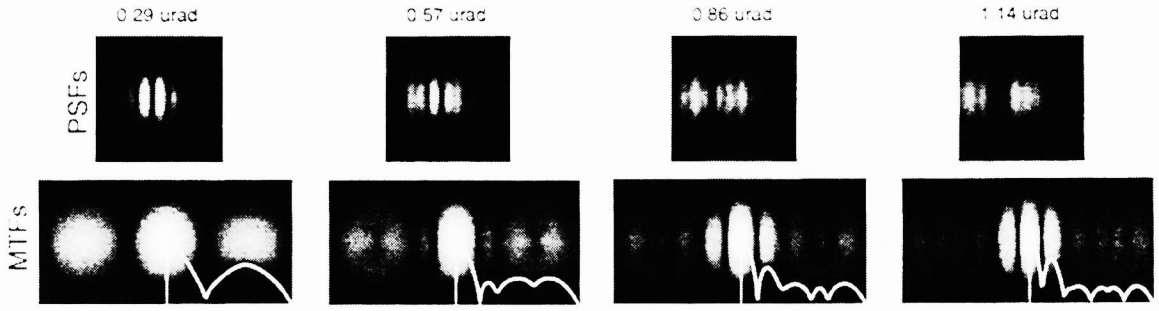


**Figure 5.** Point spread functions of the LBTI vs. tilt error along the baseline direction for one telescope beam at 4.8$\mu$m. The corresponding MTFs are shown in the lower panel.

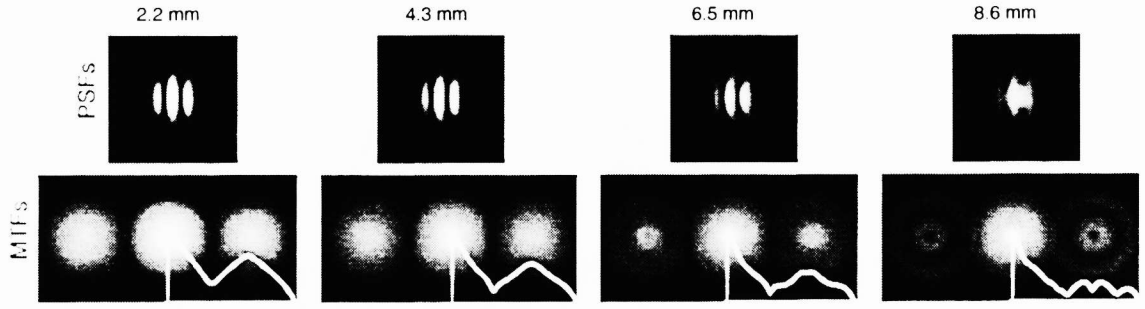


**Figure 6.** Point spread functions of the LBTI vs. defocus error in one telescope beam. The resulting curved fringes could be used to establish initial alignment. The corresponding MTFs are shown in the lower panel.

Figure 6 illustrates the effects of a focus error in one aperture. Since the defocus term is only in one aperture, it is offset from the origin by $\delta x$, having the form $2\pi*((x-\delta x)^2+y^2)$. Since the first part can be written as $x^2-2*\delta x*x+\delta x^2$, it can be seen that the resulting image will have a focus error($x^2$), a tilt error ($2*\delta x*x$) and a piston error ($\delta x^2$) from this effect. These errors combine to form curved fringes which change orientation on either side of focus, providing a possible diagnostic for adjusting focus between the two apertures.

Again, the separation of the Airy patterns leads to a reduction of the PSF maximum by at least a factor of four, but unlike the tilt cases, the defocus error will not stabilize at this value, due to the additional shifting of the cosine envelope. For the same reason, the double-aperture structure of the PSF is not seen as strongly in this case, since the Airy pattern peaks are severely attenuated. Accordingly, the width of the MTF is broader than for the tilt case.

## 2.3. LBTI Merit Functions

The merit function should describe the quality of the above PSFs in a simple way. Considering traditional merit functions, such as Strehl ratio and the MTF cutoff, led us to explore new merit functions, more appropriate to the LBTI configuration.

The traditional Strehl ratio compares the height of the PSF at the chief ray with the height of the PSF at the chief ray in the absence of all aberrations. However, for the LBTI, the peak of the PSF may not occur at the chief ray location, but instead may occur where the maxima of the cosine and Airy patterns overlap. The case of 0.5 waves of piston, shown in Figure 7, illustrates this well. The traditional Strehl ratio for this pattern is zero. However, the fringes are of good quality, with high contrast and maxima.

For the LBTI, it is crucial that such cases are not falsely excluded by the merit function. A quantity similar to the Strehl ratio, but following the peak of the PSF rather than the chief ray, would correctly include such acceptable PSF's. This new quantity, termed "peak Strehl", is defined as the ratio of the maximum of the aberrated PSF to the maximum of the unaberrated PSF. It is independent of the location of the chief ray.

The peak Strehls for the first-order aberrations in the LBTI system are shown in Figure 8. The plots show the physical behavior of the PSFs, discussed above, showing that piston reduces the peak by a factor of two, tilts

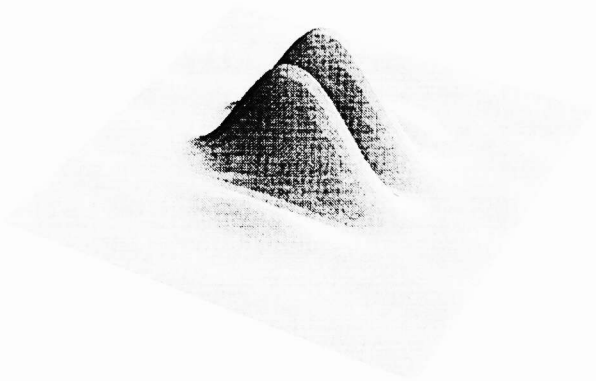

**Figure 7.** Surface plot of the PSF at the combined focus of the LBT with 0.5 waves of piston error in one telescope beam at 4.8$\mu$m. In this case the traditional Strehl ratio equals zero whereas the peak Strehl is 0.85.

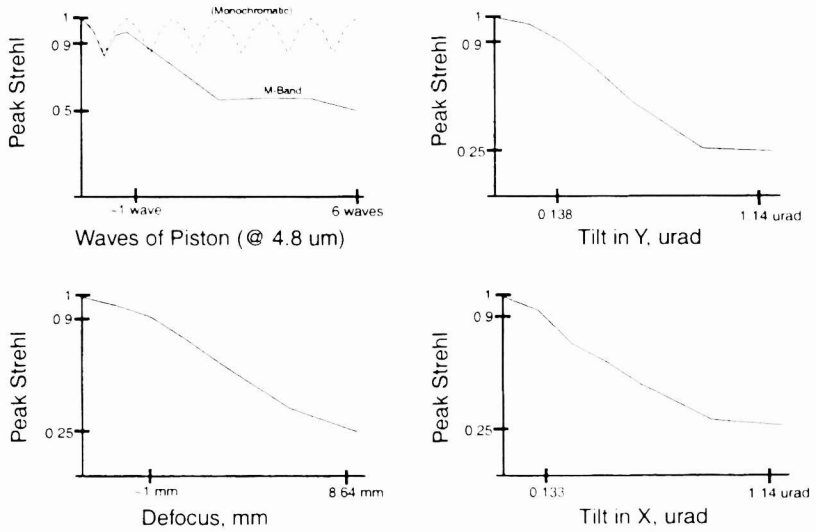


**Figure 8.** Peak Strehl ratios for the first-order aberrations in the combined image from the LBTI at 4.8$\mu$m.

by a factor of four, and defocus by any factor. The slightly more rapid decline of the PSF peak for tilt errors perpendicular to the cosine fringes also appears. For the case of 0.5 waves of piston error (Figure 7), the peak Strehl is 0.85 compared to the traditional Strehl ratio which would be zero.

From Figures 3 through 6, it is seen that the MTF has two major features that change with aberrations: the width of the central peak, and the height of the secondary peak. A second good merit function for the LBTI may then be the normalized sum of the height of the MTF at two frequency locations, the first being the frequency for which the center peak of the unaberrated MTF has a height of 0.5, and the second being the frequency for which the maximum of the secondary peak in the unaberrated MTF occurs. Again, this merit function would correctly identify the test case of 0.5 waves of piston as a "good" system.

Fringe contrast, or visibility, is not a useful merit function for the design phase of the LBTI beam-combiner.It is more useful when tolerancing and positioning the beam-combiner elements. However, maximizing visibility is equivalent to maximizing the peak Strehl.

## 2.4. Peak Strehls in the LBTI

If the peak Strehl is taken to be the merit function of the LBTI system, and acceptable systems have a peak Strehl value of 0.9 or higher, then the tolerable amount of the first order aberrations for the LBTI can be taken directly from Figure 8, as summarized in Table 1.

**Table 1.** Tolerable Positioning Errors in the LBTI at 4.8$\mu$m

| ABERRATION | MAX FOR PEAK STREHL = 0.9 |
|---|---|
| Piston | 1 wave (4.8$\mu$m) |
| Defocus | 1 mm (f/15.0) |
| Tilt (perpendicular to baseline) | 0.14 $\mu$rad (0.028 arcsec) |
| Tilt (along baseline) | 0.13 $\mu$rad (0.027 arcsec) |

These limits apply to the case in which one aperture is aberrated and the other is not, so that one Airy pattern is always coincident with the cosine envelope. For the general case in which both are aberrated with respect to the cosine envelope, the constraints will be slightly tighter, depending on the exact form of error propagation in the system.

# 3. OPTICAL DESIGN TOOLS

Multi-aperture entrance pupil optical systems, such as the LBTI, present a new challenge for optical design software. Presently, commercial optical software packages provide many useful tools including optimization for the design of sequential element systems but do not adequately analyze non-sequential systems or phased multi-apertures. Conversely, stray light analysis programs provide full non-sequential wavefront propagation including diffraction effects, but due to the complexity of the calculations, do not provide optimization routines. We have experimented designing the beam-combiner with a variety of optical software tools such as ZEMAX (Focus Software), Optima (Lockheed/Martin) and ASAP (Breault Research) and found no one tool capable of satisfying all design requirements.

Our present method of designing the LBTI beam-combiner uses one of the two optical channels and calculates optical path length in the combined image plane for various field positions in the ZEMAX merit function. We have additionally calculated the combined image tilt. In this manner, we have been able to utilize the merit function's minimum RMS wavefront default optimization with additional constraints on final focal ratio, converging beam angle (sine condition), and the combined phase and tilt. Although we are still experimenting with this method, utilizing geometrical optical design tools for phasing appears encouraging. To verify this method of design, we further export the ZEMAX files into ASAP and combine both telescopes and beam-combiners into one integrated design. The non-sequential, full wavefront propagation in this program has very powerful analysis features which allow independent verification of the combined telescope design.

To test the above design procedure, we analyzed a design involving a single relaying ellipse. We first optimized the ellipse's conic for minimum RMS wavefront error and then optimized using our improved method. The combined PSFs of these two methods were compared in ASAP. Our method improved the combined point spread functions and extended the field as shown in Figure 9. At 1.0 arcmin field radius, the PSF on average was improved by 2% with a maximum improvement of 12.9% (cf., Figure 14). However, the phased design introduced asymmetry not seen in the non-phased design and the on-axis PSF was no longer the maximum over the field, which may have negative consequences for nulling interferometry. This issue is still under investigation.

# 4. BEAM-COMBINER REQUIREMENTS

In the following optical design studies, our goal is to maximize the LBT's interferometric capabilities in the thermal infrared and to accomodate the widest possible field of view for future use. Consequently, we are exploring all-reflective designs which reimage the telescope focal plane onto a detector and which also image the telescope pupil onto an internal cold stop. This minimizes background contamination and provides a location for future, higher density, deformable mirrors. Table 2 summarizes the optical parameters of the LBT which we assume for this design.

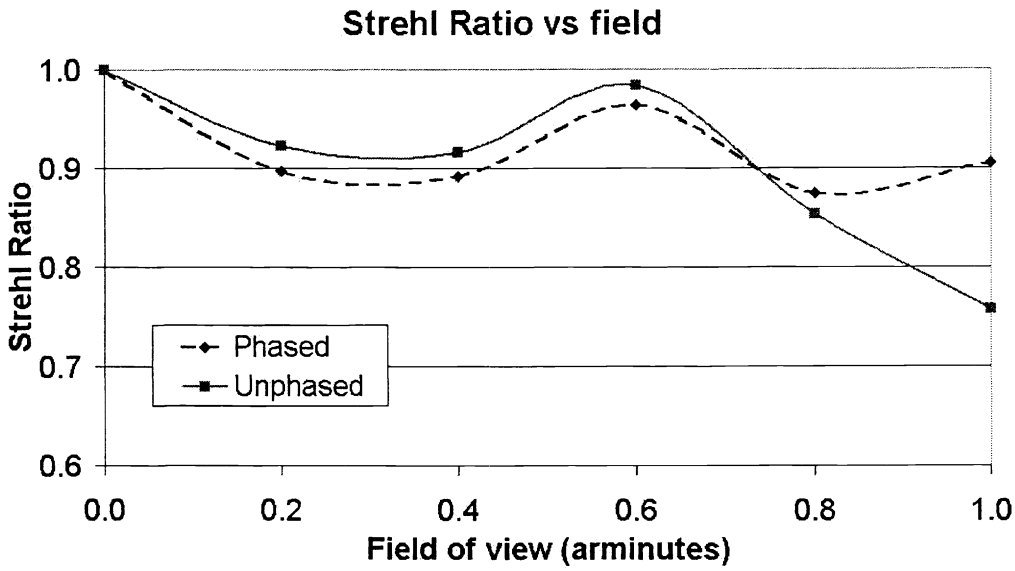


**Figure 9.** Comparison of results from different optimization techniques in ZEMAX. For the "phased" curve the conic constant of the ellipsoidal reimaging mirror was optimized for minimum phase error and for wavefront quality. In the "unphased" case only wavefront quality was considered. For a field of 1.0 arcmin radius along the baseline direction, the PSF was improved as much as 20%.

**Table 2.** Optical Specification of LBT f/15 Gregorian Foci with Adaptive Optics

| | |
|---|---|
| Parabolic primary clear aperture (D) | 8.25 m |
| Primary focal ratio | 1.1418 |
| Central obstruction | 0.898 m |
| AO secondary diameter (STOP) | 0.91 m |
| AO secondary conic | -0.7328 |
| Separation of primary-secondary | 10.66369 m |
| Back focal distance | 3.050 m |
| System focal ratio | 15.00 |
| Platescale | 1.67 arcsec $mm^{-1}$ |
| Unvignetted field of view | 4 arcmin |
| Center-to-center baseline (S) | 14.417 m |
| Edge-to-edge baseline (B) | 22.667 m |

### 4.1. Optical & Geometrical Effects

The individual telescope and beam-combiner optics must obey several fundamental geometrical principles to produce a high combined-beam Strehl ratio over a field. First, the individual telescope beams must have the highest possible Strehl ratio to optimize the performance of nulling interferometry and to obtain the highest signal-to-noise imaging. Each of the LBT's adaptive secondaries is designed to provide a Strehl ratio of $\geq$0.9 in the $K$-band over an unvignetted field of view of 4 arcmin diameter.

Second, the individual image centers must be almost perfectly coincident. At 4.8$\mu$m, the images must overlap to within 0.03 arcsec to achieve a peak Strehl ratio of 0.9 in the combined image (cf., Figure 8). At a radial distance of 1.0 arcmin, the two focal plane scales must then match to 0.05%.

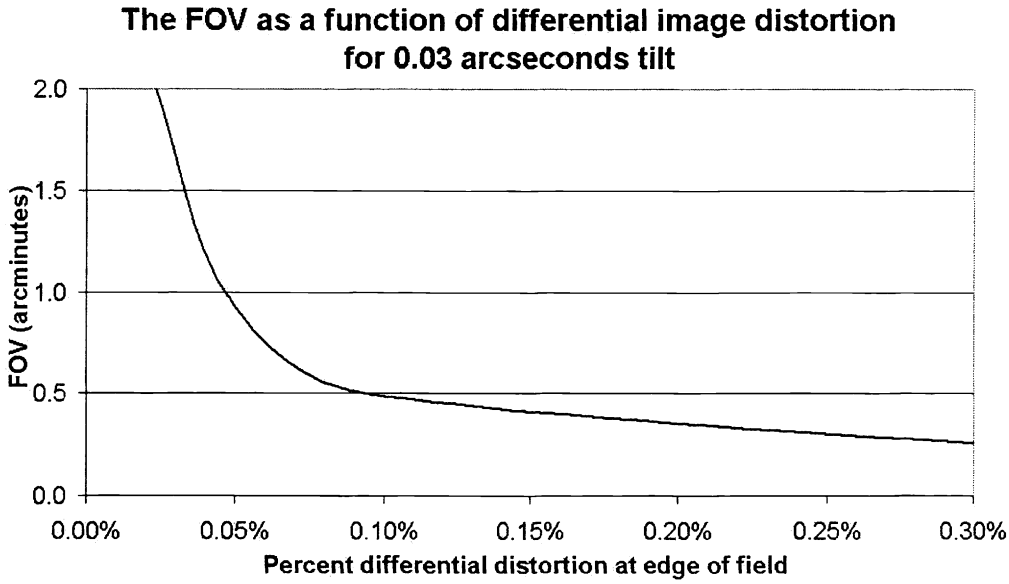


**Figure 10.** Allowable differential distortion versus half-field of view for an assumed error in image overlap of 0.03 arcsec at 4.8 $\mu$m.

A third requirement, the sine condition, has broad implications. At each point in the field, the apparent geometry of the exit pupil must match that of the entrance pupil. In other words, the scales which characterize the images and the fringes must be identical at every point in the field or else the fringes, which are localized because of their finite coherence length, will not be centered in the combined image. Thus, the optical distortions associated with the individual images and the fringes must be identical to a one fringe width at the edge of the field. At 4.8$\mu$m, as shown in Figure 10, the maximum allowable single beam distortion at 1.0 arcmin off-axis is 0.1%. The maximum "differential distortion" (distortion matching between the two beams) is 0.05%. The fringe scale depends on the convergence angle between the two incoming beams and must also be accurate to 0.1%. Figure 11 illustrates the trade-off between adherence to the sine condition and the amount of differential piston error for a given field of view.

## 4.2. Polarization Effects

To achieve precise cancellation of starlight in nulling interferometry, the two interfering beams must have the same polarization properties. For this reason, even at 10$\mu$m wavelength, the beam-combiner must use the central combined focus station, instead of the lateral beam-combiner positions. The light travelling through the LBT has two 45 degree reflections prior to beam combination. If the beam-combiner is on-axis, the sense of polarization in the plane of incidence for both beams is identical. However, if the beam-combiner is off-axis or has out-of-plane reflections, this symmetry is broken. Light propogating through the left beam in the plane of incidence will interfere with light which has components both in the plane of incidence and perpendicular to it, for the right beam. The component in the plane of incidence has no relative phase shift to the left beam. The component perpendicular to it has a phase difference from the left beam. This causes a reduction in the visibility. For regular interferometry this reduction is negligible even at the lateral stations (V=0.98 at 1.25 $\mu$m). For nulling interferometry it would result in a 0.06% residual at 10 $\mu$m and be a dominant source of starlight leak.

## 4.3. Choice of Final Focal-ratio

In the following optical design we have chosen the final focal ratio of the indivdual beams to be f/41.2 with an outer envelope of f/15. Although not a requirement, this focal ratio is desirable for two reasons. First, as shown in Table 3 for both near- and mid-infrared wavelengths, a ~3:1 magnification of the plate scale of the individual telescopes allows modern detector pixel sizes to nearly Nyquist sample the fringe width ($\lambda$/B), where B is the edge-to-edge diameter of the LBT. Thus, at these wavelengths, the beam-combiner also serves as the camera optics, simplying

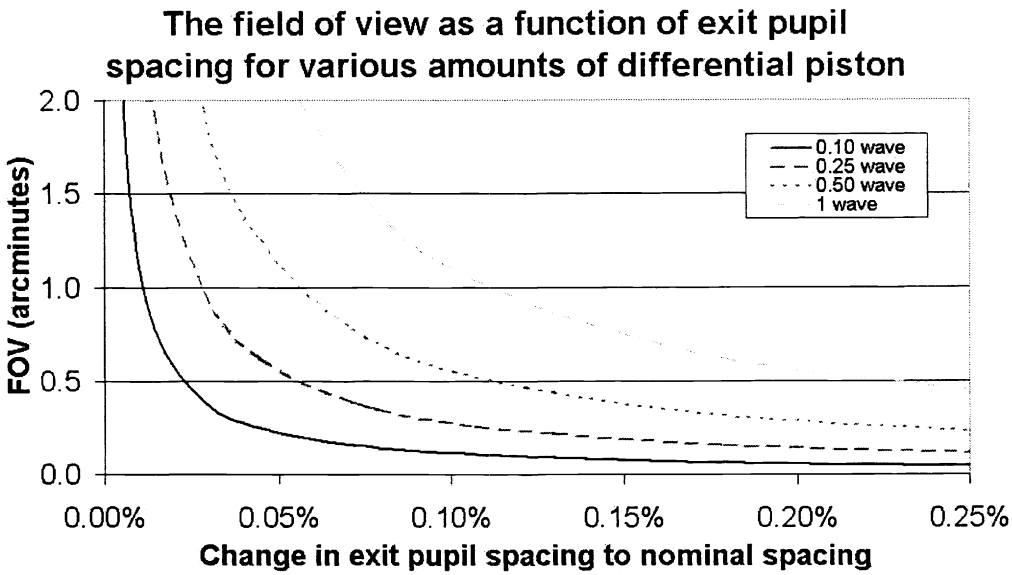


**Figure 11.** Quantitative study of the trade-off of differential piston error vs. error in the sine condition for different half fields of view at 4.8$\mu$m.

**Table 3.** Angular Resolutions vs. Wavelength

| Wavelength | $\lambda$/D | $\lambda$/S | $\lambda$/B | Pixel Size | Magnification |
|---|---|---|---|---|---|
| J (1.25 $\mu$m) | 31.3 mas | 17.9 mas | 11.4 mas | 18.5 ($\mu$m) | 5.4 |
| H (1.65) | 41.3 | 23.6 | 15.0 | 18.5 | 4.1 |
| K (2.2) | 55.0 | 31.5 | 20.0 | 18.5 | 3.1 |
| L (3.4) | 85.0 | 48.7 | 31.0 | 18.5 | 2.0 |
| M (4.8) | 120 | 68.8 | 43.7 | 18.5 | 1.4 |
| N (10) | 250 | 143 | 91.0 | 75 | 2.9 |
| Q (20) | 500 | 286 | 182 | 75 | 1.4 |

the optical design for first-light. Second, instruments at the LBT's individual f/15 foci can then also be used at the combined focus while still Nyquist sampling the telescope cut-off frequency.

## 5. ROLE OF ADAPTIVE SECONDARY MIRRORS

Table 4 summarizes the performance capabilities of the adaptive Gregorian secondary mirrors. In median seeing with moderate wind speeds (20-30 m sec$^{-1}$), they are expected to yield images with a Strehl Ratio of $\geq$0.9 in the $K$-band. An important feature of these mechanisms is an internal servo-loop controlling the absolute position of each actuator. Their spatial positioning accuracy (1 nm), stroke, (100 $\mu$m), and rapid response time ($\leq$1 msec) enable them to compensate for several forms of pathlength and wavefront tip/tilt fluctuations, thereby greatly simplifying the design of the beam-combiner. These advantages are as follows:

1). The two mirrors can be pistoned differentially for pathlength correction. A piston motion of each mirror by 1 $\mu$m in opposite directions yields a 4 $\mu$m change in relative pathlength without significantly modifying the intrinsic image quality. 2). Piston motions of the secondaries can actively (1 kHz) control atmospherically induced pathlength differences ($\sim$30 $\mu$m peak-to-valley across the LBT baseline. Simultaneous figure corrections can compensate for associated changes in spherical aberration and focus. 3). The secondaries can be actively "slewed" ($\sim$20 $\mu$m sec$^{-1}$) for locating and scanning the zero-phase position. 4). They can provide active (1 kHz) control of vibration-induced

pathlength fluctuations. 5). Slow piston motions of the secondaries provide for open-loop correction of pathlength changes caused by telescope mecahnical flexure and temperature changes.

**Table 4.** Performance Specifications of the f/15 Adaptive Optics Deformable Secondary Mirror

| | |
|---|---|
| Number of actuators | 918 |
| Actuator spacing on primary | ~230 mm |
| Actuator stroke | 100 $\mu$m |
| Actuator resolution | 1 nm |
| Actuator settling time (90%) | $\leq$1 ms |
| System internal closed-loop frequency | 40 kHz |
| System closed-loop frequency | 1 kHz |

Details of these mirrors and the complete adaptive optics system are provided by several papers at this conference (Gallieni et al. 2000; Del Vecchio & Gallieni 2000; Carbillet et al. 2000).

## 6. A 2-20 MICRON INTERFEROMETER FOR FIRST-LIGHT

### 6.1. The Thermal-IR Beam-Combiner

Based on the principles and constraints summarized in the previous sections, we are evaluating several all-reflective designs for a thermal-IR beam-combiner which can direct a phased field of view quickly to different, co-mounted science instruments. For wavelengths of 2-20 $\mu$m this beam-combiner is relatively simple, requiring no complicated mechanisms or metrology systems. Although occupying a large evacuated volume, the optical components are relatively compact and will not require an unusually large cooling system. In the following we consider one of several optical designs now under study.

Table 5 and Figure 12 summarize a potential thermal-IR beam-combiner for first-light. The optics of each interferometric arm feature a single off-axis ellipsoidal mirror to reimage the telescope focal plane at a magnification of 2.75:1, forming a cold pupil on one of the folding flats. The exit pupil is demagnified a factor of 5.7 and is located 6.56 m before the focal plane. The radius of the ellipsoidal mirror was chosen for best imaging over the field as shown in Figure 13. All other elements are unpowered fold flats and represent one combination for minimizing the volume of the dewar. The optical distortion at 1.0 arcmin off-axis is 0.01% along the baseline direction and 0.06% in the perpendicular direction.

Combined PSFs at the focal plane over a 2 arcmin diameter field in the $M$-band are compared in Figure 14 with an example of the combined on-axis PSF. Each block represents the PSF at various 0.5 arcmin field points. We believe the low Strehl value at the bottom of the bottom of the field is caused by asymmetry of the design as well as difficulties in optimization. We are confident that we can improve the results for all field points. The MTF degradation as a function of field is plotted in Figure 15.

Analytical values for the requirement of maintaining the sine condition are very tight. This calculation is the requirement on how accurately the exit pupil positions must be maintained. Figure 11 depicts the half field of view as a function of exit pupil positioning for various amounts of allowable differential piston error at $M$-band. A 0.10% change in exit pupil spacing corresponds to a stabilization of 280 $\mu$m over 280 mm.

### 6.2. Science Instruments

The thermal-IR beam-combiner described above can feed different scientific instruments as shown schematically in Figure 16. Several different instruments can be co-mounted simultaneously and fed by different dichroic mirrors. Each of these instruments would need its own tip/tilt and phase sensors to interface to the adaptive secondary mirrors. In addition, each instrument should be mounted on a rotatable flange to compensate for field rotation in both the science field and in the fields of the tip/tilt and phase sensors. Such a rotating interface may necessitate specific optical windows so that the beam-combiner and instruments share different vacuums.

The 8-14 $\mu$m nulling interferometer would lie directly under the beam-combiner on the optical axis. The dichroic mirrors above it should be retractable to reduce effects of scattered light, induced color, and aberrations.

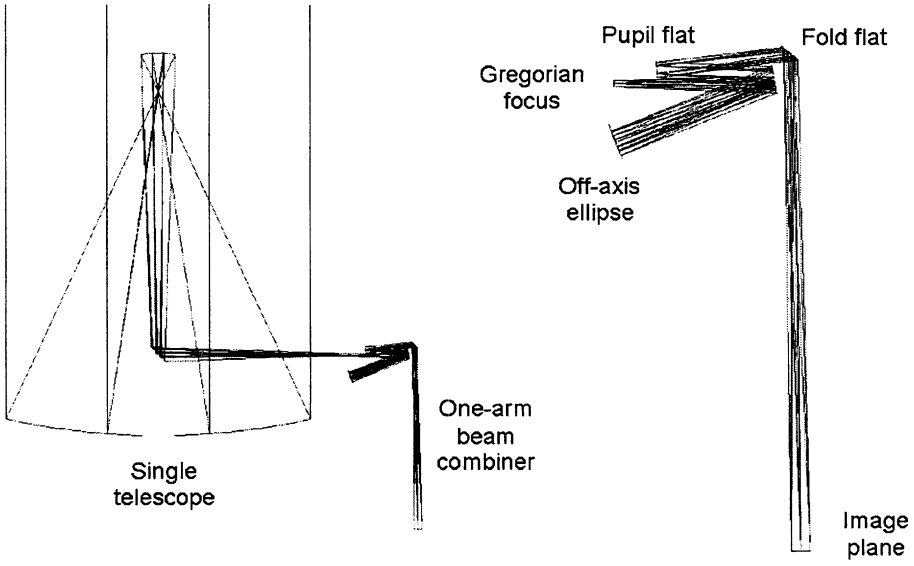


**Figure 12.** Optical schematic of one arm of the cryogenic beam-combiner.

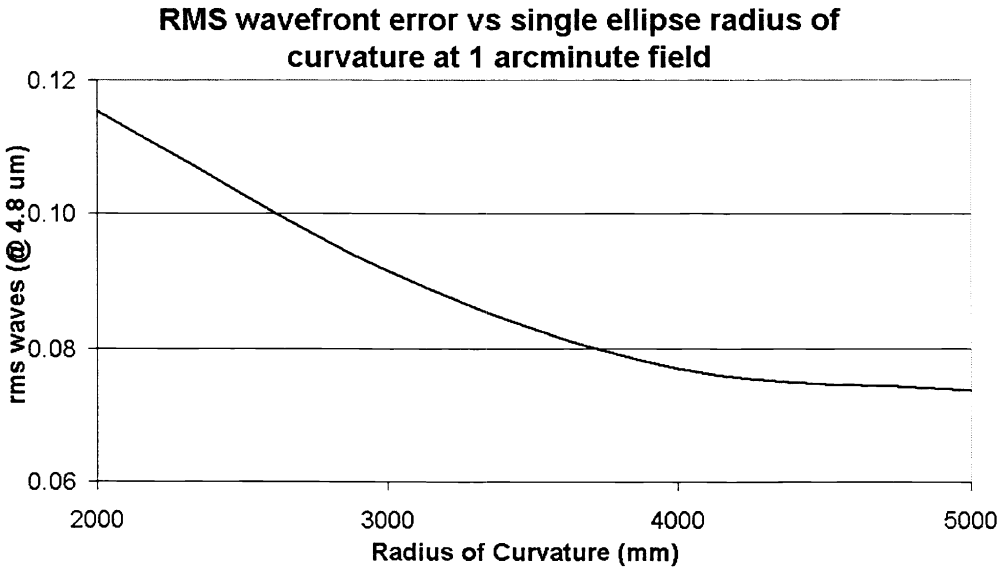


**Figure 13.** RMS wavefront error vs. radius of curvature for an elliptical reimaging mirror. The image quality of the reimaged focal plane is plotted for a wavelength of 4.8 $\mu$m at the edge of a 1.0 arcmin radius field.

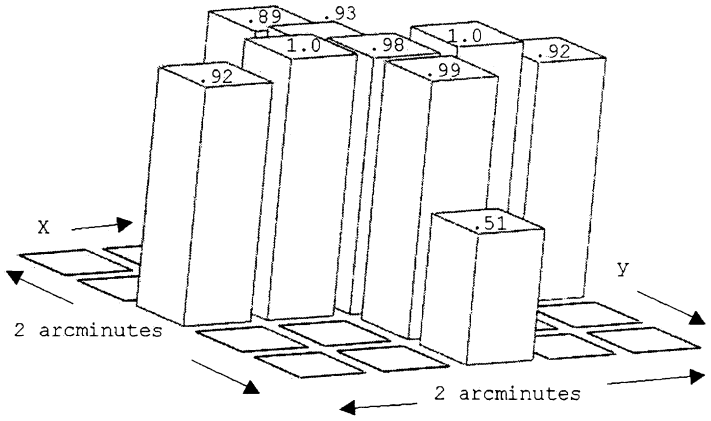


**Figure 14.** A two dimensional representation of the PSF at various field points at the combined focal plane. Neighboring field points are 0.5 arcmin in separation. The y-axis lies along the baseline direction.

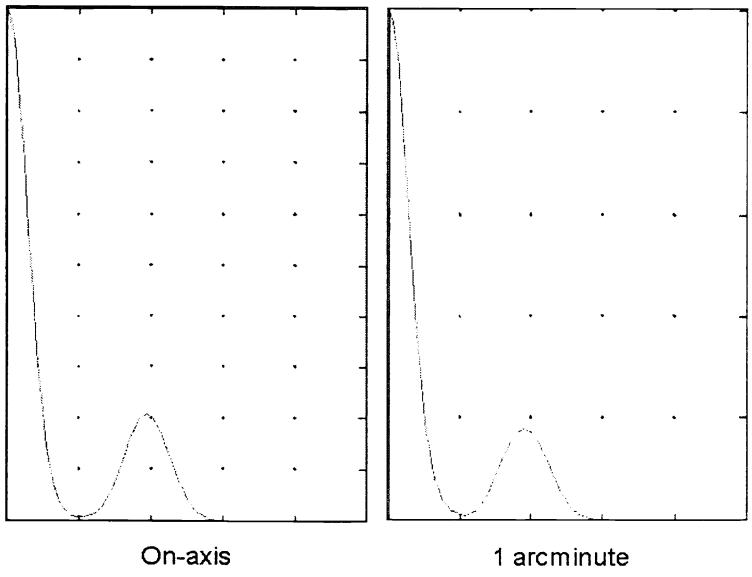


**Figure 15.** Modulation transfer functions for on-axis and 1.0 arcmin off-axis images at 4.8$\mu$m from the beam-combiner design shown in Figure 12.

**Table 5.** Specifications of a First-Light, All-Reflective Beam-Combiner for the LBT

| | |
|---|---|
| Focal ratio (single beam) | 41.208 |
| Focal ratio (combined beams) | 15.00 |
| Sine condition angle (center-to-center) | 2.429 deg |
| Radius of ellipsoid | 5.000 m |
| Conic of ellipsoid | -0.0823178 |
| Off-axis distance of ellipsoid | 480.055 mm |
| Internal cold pupil diameter | 160.1 mm |
| Magnification of exit pupil | 5.7 |
| Distance of exit pupil from focal plane | 6.566 m |
| Combined beam focal plane scale | 0.607 arcsec $mm^{-1}$ |

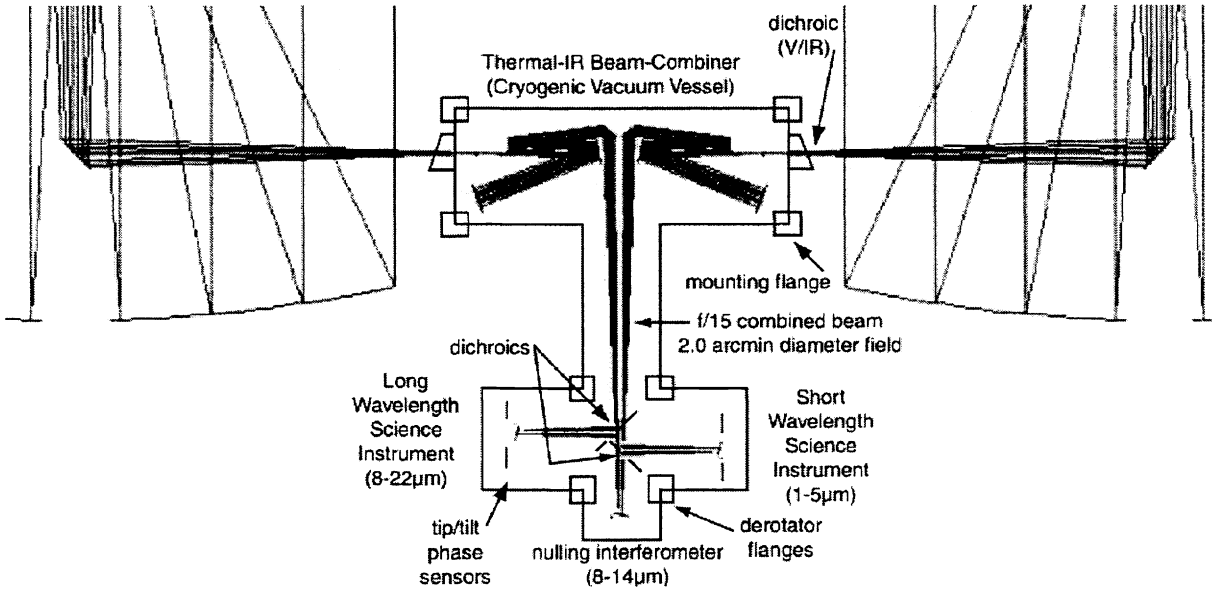


**Figure 16.** Schematic concept design of the thermal-IR beam-combiner and attached science instruments.

## 6.3. Tip/tilt and Phase Sensors

From the discussion in Section 2.2, the tip/tilt fluctuations in the wavefronts from the two telescope beams must be measured and corrected to very high precision. The absolute, as well as the relative, position of each image must be stabilized to ~0.03 arcsec. To achieve this accuracy a guide star in the field is required within 1-2 arcmin of the on-axis science object (Sandler et al. 1994). To increase the likelihood of finding such a star and to measure its centroid with the highest possible accuracy, a high speed, near-IR (1-2 $\mu$m) detector should be located as close as possible to the final science detector. This location will help minimize effects of differential flexure and optical aberrations in the beam-combiner and science instrument.

A similar argument applies to the pathlength sensor which is required for stabilizing the fringes at the combined focus. Pathlength fluctuations must be tracked and removed dynamically through observations of an off-axis guide star. Theoretical modeling studies by Esposito et al. (2000) indicate that the isopistonic angle for a pathlength fluctuation of 0.1$\lambda$ is ~30 arcsec at a wavelength of 4.8$\mu$ for an outer scale of turbulence of 80m (Lloyd-Hart et al.

1995).

A possible model for these sensors is under construction for the ARIES instrument (Sarlot et al. 1999) on the 6.5 m MMT. Here a probe mirror and detector travel within the dewar on a stiff (x,y)-translation stage to access field stars over a 100 arcsec diameter field (50 mm) for tip/tilt and focus measurements. Such a design might be modified to include separate channels for the two tip/tilt measurements and also for examining the fringe position/contrast in the combined image. This sensor mechanism should be duplicated within each science instrument at the LBT combined focus.

A crucial aspect of this approach is the development of high speed, very low noise detectors for the near-IR. ARIES will use a HAWAII detector operating in a subarray readout mode with multiple sampling. In an 8x8 pixel subarray Weigelt (1999) has acheived a readnoise of 8 RMS electrons. Lower readnoise and higher quantum efficiency detectors are desired for this application.

## 7. FUTURE WORK

Additional research is needed to understand how the various alignment and manufacturing errors combine to impact the overall beam-combiner system. The modeling techniques discussed here should be extended to include an "error budget" for optimizing the beam-combiner parameters. Other all-reflective beam-combiner designs should also be evaluated in an effort to provide the highest performance and most versatile concept.

## ACKNOWLEDGMENTS

The authors acknowledge the generous assistance of Dr. Joe Shiefman and Breault Research Organization with the implementation of the ASAP software tool and of the optics group at Lockheed with the use of the OPTIMA package. Phil Hinz and Erin Sabatke acknowledge support through the Michelson Graduate Fellowship program. This effort has been supported by resources made available through the Director of Steward Observatory.

## REFERENCES

1. Hill, J.M., & Salianri, P., 2000, Proc. SPIE, 4004, paper 07, in press
2. Angel, J.R.P., Hill, J.M., Strittmatter, P.A., Salinari, P., & Weigelt, G., 1998, Proc. SPIE, 3350, 881
3. Hill, J.M., 1994, Proc. SPIE, 2200, 248
4. Lloyd-Hart, M., 2000, PASP, 112, 264
5. Hinz, P., Angel, R., Hoffmann, W., McCarthy, D.W., McGuire, P., Cheselka, M., Hora, J., & Woolf, N., 1998, Nature, 395, 251
6. Hinz, P.M., Angel, J.R.P., Woolf, N.J., Hoffmann, W.F, & McCarthy, D.W., 2000, Proc. SPIE, 4006, paper 38, in press
7. Byard, P. & Bonaccini, D., 1994, Proc. SPIE, 2200, 446
8. Salinari, P., 1996, Proc. SPIE, 2871, 564
9. Herbst, T.M., Rix, H.W., Richichi, A., & Gai, M., 2000, Proc SPIE, 4006, paper 82, in press
10. Walker, C., d'Aubigny, C., Hill, J.M., & Burge, J., 2000, Proc SPIE, 4015, paper 30, in press
11. Gallieni, D., Del Vecchio, C., Anaclerio, E., & Lazzarini, P.G., 2000, Proc SPIE, 4007, paper 08, in press.
12. Del Vecchio, C. & Gallieni, D., 2000, Proc SPIE, 4007, paper 09, in press
13. Carbillet, M., Correia, S., Femenia, B., & Riccardi, A., 2000, Proc. SPIE, 4007, paper 56, in press
14. Sandler, D.G., Stahl, S., Angel, J.R.P., Lloyd-Hart, M., and McCarthy, D. 1994, J. Opt. Soc. Am. A, 11, 925,
15. Sarlot, R., Burge, J., & McCarthy, D., 1999, Proc SPIE, 3779, 274
16. Esposito, S., Riccardi, A., & Femenia, B., 2000, A&A, 353, L29
17. Lloyd-Hart, M. et al., 1995, ApJ, 439, 455
18. Weigelt, G., 1999, private communication